AUT Journal of Electrical Engineering

AUT J. Elec. Eng., 57(3) (2025) 485-498
DOI: 10.22060/eej.2025.23758.5633

# Evaluation of Lightning Multiple Strokes Nature on Aircraft Avionic Equipment Performance Based on TLM

Hamed Neyshabouri * [1,2], Mohsen Niasati [2]

[1] Faculty of Electrical and Computer Engineering, Semnan University, Semnan, Iran.
[2] Department of Electrical Engineering, National University of Skills ( NUS ), Tehran, Iran.

**ABSTRACT:** The phenomenon of lightning is a highly intricate natural occurrence characterized by the rapid discharge of electricity in the atmosphere. Understanding the intricacies of lightning encompasses a range of scientific disciplines, including meteorology, physics, power engineering, and environmental science. Lightning inductive effects can result in undesired operation of the avionic equipment and endanger flight safety. This paper analyzes the multiple-stroke nature of an actual flash for evaluating the indirect effects properly, such as coupling into the interior equipment of an aerospace vehicle. To the best of our knowledge, subsequent strokes in the flash tend to have a higher rate of rise and lower crest amplitudes, compared to the initial stroke. The metallic aircraft structure acts as a full Faraday cage, while composite materials can decrease the electromagnetic shielding efficiency of the original metal body. The time domain finite element analysis based on the transmission line model method is regarded as a numerical technique to solve field problems by implementing circuit equivalents. The objective of this study is to examine the characteristics associated with lightning strikes by the MIL-STD-464A standard. It also aimed to simulate the induced current in coaxial cables, surface current density, and electric and magnetic field strength by integrating Matlab and CST software.

**Review History:**

Received: Dec. 16, 2024
Revised: Apr. 27, 2025
Accepted: Jul. 22, 2025
Available Online: Oct. 20, 2025

**Keywords:**

Lightning
Subsequent Strokes
Avionic
Composite
Coaxial Cable

## 1- Introduction

Aircraft flight safety can be affected by various atmospheric disturbances, with lightning being one of the most significant. Lightning is a natural electrical discharge that typically occurs within cumulonimbus clouds during precipitation. It can adversely affect aircraft systems and equipment, leading to malfunctions, failures, or incorrect data readings. Lightning strikes pose both direct and indirect threats. Direct effects include physical damage such as pitting, melting of aircraft surfaces, and the ignition of fuel vapors [1]–[6]Carbon Fiber Reinforced Plastics (CFRP. Indirect effects involve electromagnetic interference with avionics, navigation systems, and other onboard electronic equipment [7]–[11]. The vulnerability of electronic systems has increased with advancements in semiconductor technology, particularly the reduction in the size of semiconductor junctions, which makes them more susceptible to electrostatic damage [12]. Smaller semiconductor junctions are exposed to some damage from electrostatic voltages. One industry that has been significantly impacted by the erratic weather patterns resulting from climate change and global warming is aviation. Climate change and global warming now have an increasing impact on weather-related aircraft accidents[13]. Lightning not only threatens aircraft in flight but also poses risks to airport operations and air traffic control (ATC) systems [14].

## 2- Significance of lightning certification

According to MIL-STD-464A [15], aircraft will meet its operational performance requirements for both direct and indirect effects of lightning. The expression of the double exponential model of the lightning current is as follows:

$$i(t) = I_0 \left\{ \exp\left(-t/\alpha\right) - \exp\left(-t/\beta\right) \right\} \quad (1)$$

Where i(t) represents the instantaneous value of lightning current, $I_0$ indicates the peak value of lightning, α shows decay time, and β is considered as rise time. Table 1 presents standard parameters for lightning currents, where a typical lightning flash consists of an initial return stroke followed by several subsequent strokes.

For protection against direct effects, a single return stroke is usually sufficient, but for assessing indirect effects, such as electromagnetic coupling in aerospace vehicles, multiple strokes must be considered, as discussed in references [15]–[17]. One can use Fig. 1 to evaluate the indirect effects of the lightning environment.

The first return stroke is typically modeled using a double

*Corresponding author's email: H.neyshabouri@semnan.ac.ir

**Table 1. Lightning current based on Mil-Std-464A.**

| Current component | Description | I(t) | | |
|---|---|---|---|---|
| | | **lightning's peak value(A)** | **decay time(s)** | rise time(s) |
| **A** | Severe stroke | 218810 | 88e-6 | 1.5e-6 |
| **B** | Intermediate current | 11300 | 14e-4 | 5e-4 |
| **C** | Continuing current | 400 for 0.5s | Not applicable | Not applicable |
| **D** | Restrike | 109405 | 44e-6 | 7.7e-7 |
| **D/2** | Multiple stroke | 54703 | 44e-6 | 7.7e-7 |
| **H** | Multiple burst | 10572 | 5.3e-6 | 5.23e-8 |

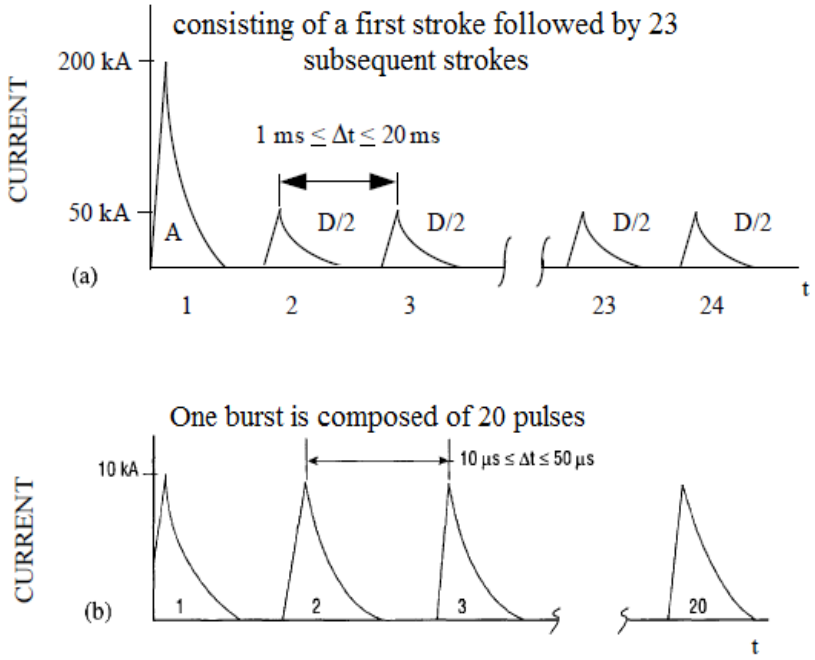


**Fig. 1. The indirect effects of lightning on the environment [15]. (a) Multiple stroke waveforms. (b) Multiple burst waveforms.**

exponential function. For subsequent strokes, the Heidler function [18] is preferred due to its more accurate and flexible representation of the waveform characteristics, making it ideal for simulating lightning surges:

$$I(0,t)=\frac{I_p}{k}*\left\{\left(\frac{t}{T_f}\right)^n/1+\left(\frac{t}{T_f}\right)^n\right\}*\exp\left(\frac{-t}{t_{au}}\right) \qquad (2)$$

Where Ip is the peak current, k is the correction factor for the peak current, t is the time, Tf is the front time constant, tau is the tail time constant, and n is the current steepness factor. Transient phenomena can be classified into various groups:

1- Temporary overvoltage transients are low-frequency transients in the range of 0.1Hz to 3 KHz

2- The switching transients class is slow front surges in the range of 60Hz to 20KHz

3- Lightning class is a fast transient in the range of 10 KHz to 3MHz

4- Restrike overvoltage is very fast front surges in the range of 10 KHz to 50MHz

Fig. 2 displays the classification of lightning entry and exit points[19]. The present study focuses on Route 1.

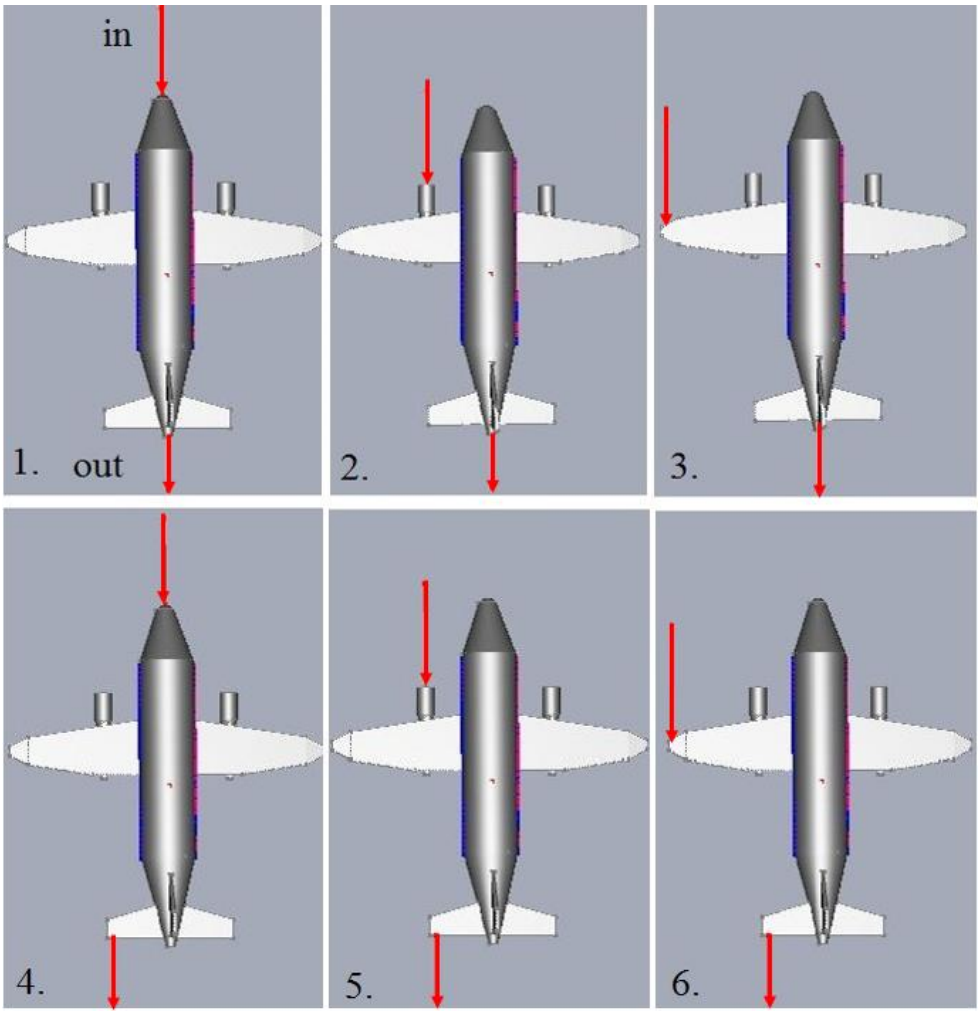


**Fig. 2. Entry and exit points of the lightning strike on an aircraft.**

## 3- Simulation of lightning

It is important to clarify that lightning is inherently a random phenomenon due to the unpredictability of its time, location, and intensity. These characteristics make lightning events difficult to model deterministically. However, for the purpose of design and simulation, particularly in aerospace contexts, deterministic models are often employed to facilitate more controlled and reproducible conditions. In our manuscript, we refer to MIL-STD-464A, a standard for lightning protection in aircraft, which provides specific lightning current waveform models. In order to evaluate the indirect effects of lightning, the number of multiple strokes usually ranges from 1-24, with a mean value of 3. Subsequent strokes in the flash tend to have a higher rate of rise and lower peak amplitudes, compared to the initial stroke. Thus, they can play a significant role in inducing voltages in aircraft wiring. To simulate lightning current and analyze the data, Matlab software was used to focus on subsequent strokes. The simulated waveform includes an initial stroke, three sections of multiple-stroke waveforms, and three sections of multiple-burst waveforms. Fig. 3 represents a simulated waveform in which the frequency ranges from 10 kHz to 3MHz.

## 4- Numerical instrument

### 4- 1- Introduction of Microstripe module

CST Microstripe is the ultimate 3D electromagnetic simulation software that employs the advanced time-domain Transmission Line Matrix (TLM) method to provide unparalleled accuracy and efficiency. This module is appropriate for structures that can function in a range with high frequency. The “Compact modeling” technique is implemented to demonstrate coupling through apertures, panels, and interaction with cabling efficiently. The Microstripe module delivers extraordinary performance for its use in the real world. A powerful Octree-based meshing algorithm represents the model details accurately, although it can decrease the cell count totally by integrating cells in less critical regions, which may lead to a more than 90% decrease in cell count, compared to basic graded-mesh techniques[20].

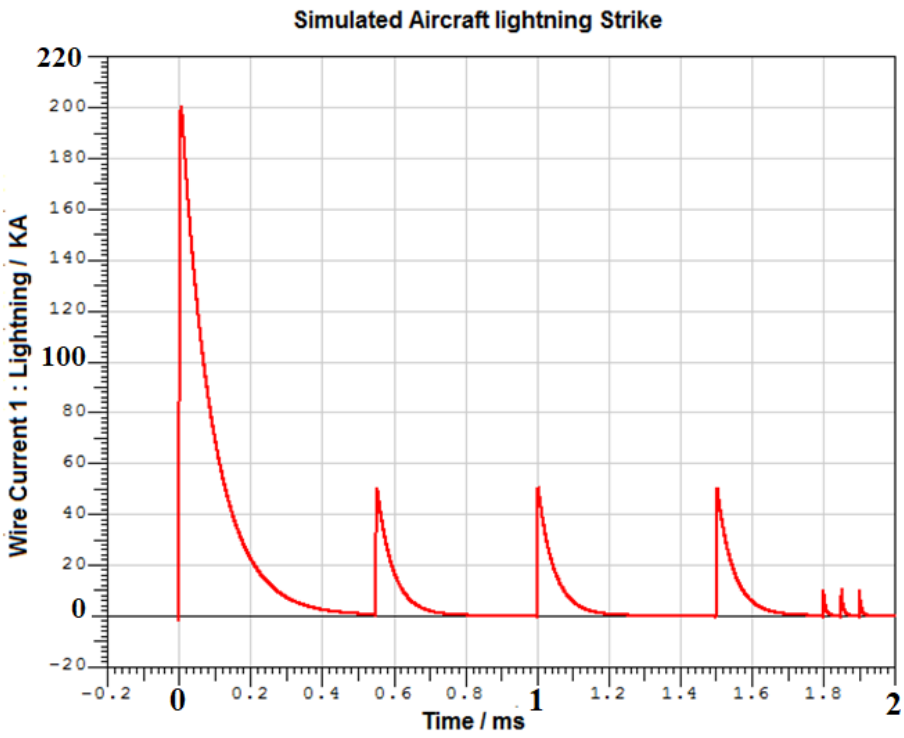


**Fig. 3. Waveform of lightning current to evaluate the indirect Effects.**

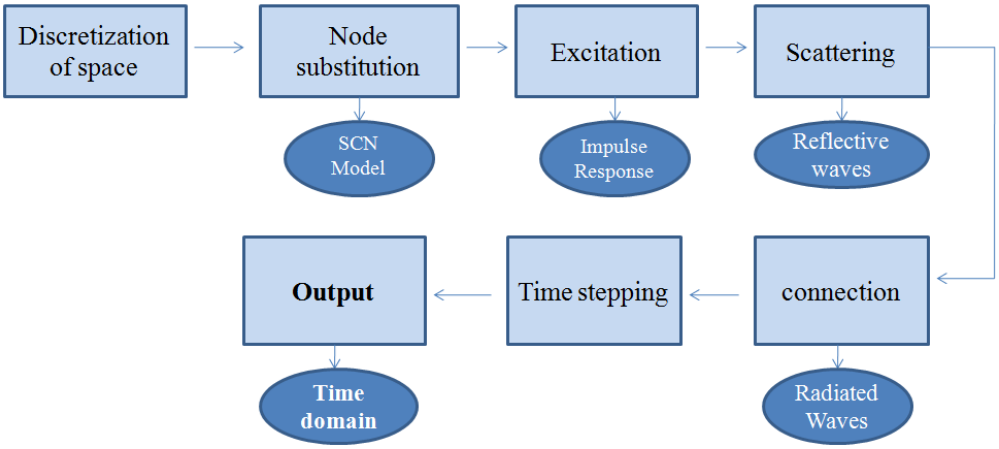


**Fig. 4. Solution steps of a problem by TLM [18].**

## 4- 2- TLM method

The transmission line matrix method is regarded as a numerical technique to solve field problems by implementing circuit equivalents. This method is based on the equivalence between Maxwell's equations and those related to voltages and currents on a mesh of continuous two-wire transmission lines. The simplicity of formulation and programming for a wide range of applications is regarded as the main characteristic of this method. The TLM method is considered a discretization process similar to other numerical techniques. Unlike mathematical discretization approaches such as finite difference and finite element methods, TLM is considered a physical discretization approach[21], [22].

Fig. 4 illustrates a schematic plan of the solution of a problem by the transmission line method.

As shown in Fig. 5, the symmetrical condensed node is considered the structure used for node substitution.

The equations governing the voltage and current behavior at each node are represented by the following differential equations [24], [25]:

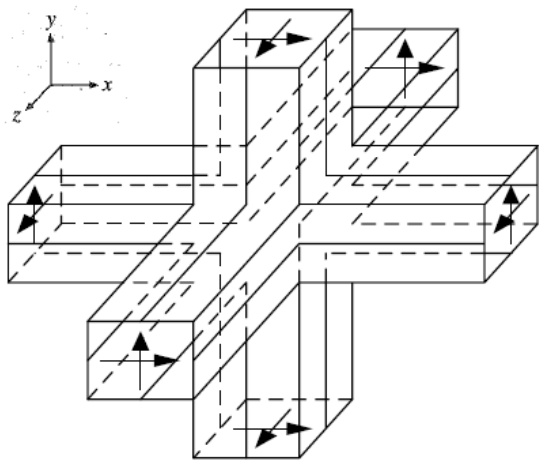


**Fig. 5. Structure of SCN model [23].**

$$
\begin{aligned}
&v\frac{\partial I_z}{\partial y}-w\frac{\partial I_y}{\partial z}=2C_x\frac{\partial V_x}{\partial t} \quad ,\\
&v\frac{\partial V_z}{\partial y}-w\frac{\partial V_y}{\partial z}=-2L_x\frac{\partial I_x}{\partial t}\\
&w\frac{\partial I_x}{\partial z}-u\frac{\partial I_z}{\partial x}=2C_y\frac{\partial V_y}{\partial t} \quad ,\\
&w\frac{\partial V_x}{\partial z}-u\frac{\partial V_z}{\partial x}=-2L_y\frac{\partial I_y}{\partial t}\\
&u\frac{\partial I_y}{\partial x}-v\frac{\partial I_x}{\partial y}=2C_z\frac{\partial V_z}{\partial t} \quad ,\\
&u\frac{\partial V_y}{\partial x}-v\frac{\partial V_x}{\partial y}=-2L_z\frac{\partial I_z}{\partial t}
\end{aligned}
\tag{3}
$$

In this context, u, v, and w represent the node dimensions along the x, y, and z axes, respectively. The inductances (Lx, Ly, Lz) and capacitances (Cx, Cy, Cz) of the transmission lines in the x, y, and z directions are considered. The currents (Ix, Iy, Iz) and voltages (Vx, Vy, Vz) correspond to the transmission lines along these axes. The relationship between the voltages, currents, and the electromagnetic fields in the solution domain can be described as follows:

$$
\begin{aligned}
&H_x=I_x/u \quad , \quad E_x=-V_x/u\\
&H_y=I_y/v \quad , \quad E_y=-V_y/v\\
&H_z=I_z/w \quad , \quad E_z=-V_z/w
\end{aligned}
\tag{4}
$$

Eq. (5) is derived by substituting Eq. (3) into Eq. (4):

$$
\begin{aligned}
&\frac{\partial H_z}{\partial y}-\frac{\partial H_y}{\partial z}=C_x\frac{2u}{wv}\frac{\partial E_x}{\partial t} \quad ,\\
&\frac{\partial E_z}{\partial y}-\frac{\partial E_y}{\partial z}=-L_x\frac{2u}{wv}\frac{\partial H_x}{\partial t}\\
&\frac{\partial H_x}{\partial z}-\frac{\partial H_z}{\partial x}=C_y\frac{2v}{uw}\frac{\partial E_y}{\partial t} \quad ,\\
&\frac{\partial E_x}{\partial z}-\frac{\partial E_z}{\partial x}=-L_y\frac{2v}{uw}\frac{\partial H_y}{\partial t}\\
&\frac{\partial H_y}{\partial x}-\frac{\partial H_x}{\partial y}=C_z\frac{2w}{uv}\frac{\partial E_z}{\partial t} \quad ,\\
&\frac{\partial E_y}{\partial x}-\frac{\partial E_x}{\partial y}=-L_z\frac{2w}{uv}\frac{\partial H_z}{\partial t}
\end{aligned}
\tag{5}
$$

As a result, it transforms into the following equation:

$$
\begin{cases}
\nabla\times E=-\mu\dfrac{\partial H}{\partial t}\\
\nabla\times H=\varepsilon\dfrac{\partial E}{\partial t}
\end{cases}
\tag{6}
$$

The scattering and connection processes are iteratively performed until they are suitable for simulating propagation over any desired time interval. During this process, voltages and currents are available at each stage. Additionally, these values represent the electromagnetic fields associated with the specific configuration and excitation of the problem at hand. The output is directly linked to the time domain.

## 5- Geometry of fuselage

In this study, the fuselage geometry is modeled based on the Airbus A320 aircraft, which features 80 windows (40 on each side). The aircraft has a total length L = 37.6 m, a wingspan W = 34 m, and an overall height H = 11.8 m. Each window has a dimension of 0.2 m x 0.3 m, as illustrated in Fig. 6. A major computational challenge arises from the disparity in structural scales: the aircraft length is 37.6 m, while the composite skin thickness is approximately 1 mm. This leads to a scale ratio of approximately L/t = 37,600, which causes numerical stiffness in traditional finite-element or finite-difference time-domain (FDTD) solvers. This issue has been addressed in previous studies[26], [27]. To manage this, CST Microwave Studio employs the compact model technique, which allows for the simplification of thin structures (such as skins or coatings) into surface impedance boundary conditions (SIBC). This approach reduces the mesh density required in the thickness direction without sacrificing accuracy. The skin depth and surface impedance of a good conductor at high frequencies are approximately given by [20]:

$$
\boldsymbol{\delta}=\sqrt{\frac{2}{\omega\mu\sigma}} \quad , \quad Z_s=\left(1/\sigma\delta\right)(1+j)
\tag{7}
$$

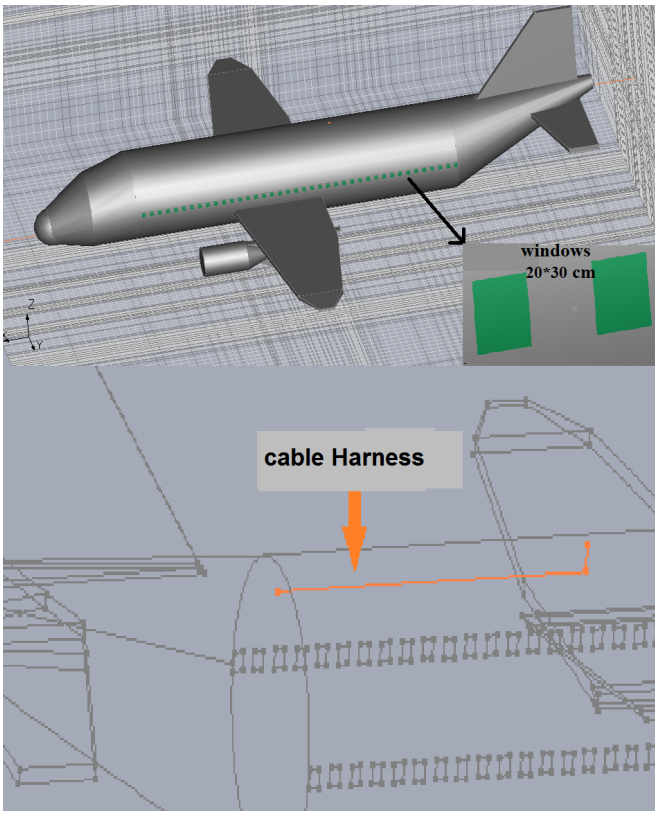


**Fig. 6. Modeled aircraft in the Simulator.**

where $\delta$ is the skin depth, $Z_s$ is the surface impedance, $\sigma$ is the conductivity $\mu$ is the magnetic permeability of the material, and $\omega = 2\pi f$ is the angular frequency. This treatment allows the simulation to remain computationally feasible while maintaining fidelity to the physical behavior of EM wave propagation and attenuation through and around structural features such as windows.

Table 2 indicates the simulation of aluminum and carbon fiber as the fuselage types in the aircraft [28].

## 6- Cable parameter

Coaxial cables, RG174, and RG-optional are evaluated as shielded cables. As shown in Table 3, the shielding properties of the cable are determined by using a transfer impedance model. Kley's formula is used for calculating the transfer impedance [29]–[33]:

$$Z_T = Z_R + i\omega L_T + (1+i)\omega L_S \tag{8}$$

Where $Z_T$ is the transfer impedance of a single braided shield, $Z_R$ is the Transfer impedance of an equivalent tube, $L_T$ is the coupling inductance, and $L_S$ is the skin inductance.

This formulation models the coupling mechanism with respect to the field penetration through the shield apertures. As illustrated in Fig. 7, the basic components of a coaxial cable, from the inside out, are the center conductor, dielectric, one or more shield layers, and an outer jacket. The cost of manufacturing coaxial cables is significantly impacted by the outer conductor or shield. RG 174 and RG-optional are terminated at 50 ohms.

## 7- Results and Discussion

To measure surface current, electric field strength, and magnetic field strength, three probes are defined at various locations as shown in Table 4.

### 7- 1- Surface current distribution on aircraft skin

Transient surface current on aluminum and carbon fiber composite (CFC) skins is illustrated in Fig. 8. As shown, surface current density at the lightning entry and exit points is significantly higher than in other regions due to the electromagnetic boundary conditions:

$$J_s = \hat{n} \times (H_2 - H_1) \tag{9}$$

Where Js is the surface current density, $\hat{n}$ is the unit normal pointing from medium1 to medium2, and $H_1$ and $H_2$ are the magnetic field intensities just below and above the surface. This relationship follows directly from Maxwell's

**Table 2. Properties of aircraft fuselages.**

| Properties | Carbon Fiber | Aluminum |
|---|---|---|
| **Relative permittivity** | 12 | 1 |
| **Relative permeability** | 1 | 1 |
| **Electric conductivity (S/m)** | 29300 in longitudinal | 3.54e+007 |
| **Thickness** | 1mm | 1mm |

**Table 3. Cable parameters.**

| Specifications | Shielded cable RG 174 | Shielded cable (optional) |
|---|---|---|
| **Inner wire diameter(mm)** | 0.48 | 0.48 |
| **Braid diameter(mm)** | 1.93 | 1.93 |
| **Filament diameter(mm)** | 0.1 | 0.05 |
| **Number of filaments in one carrier** | 5 | 4 |
| **Number of carriers** | 16 | 8 |
| **Transfer resistance(Ω/m)** | 0.0327191 | 0.3391833 |
| **Transfer inductance(H/m)** | 5.99e-10 | 4.4015e-8 |

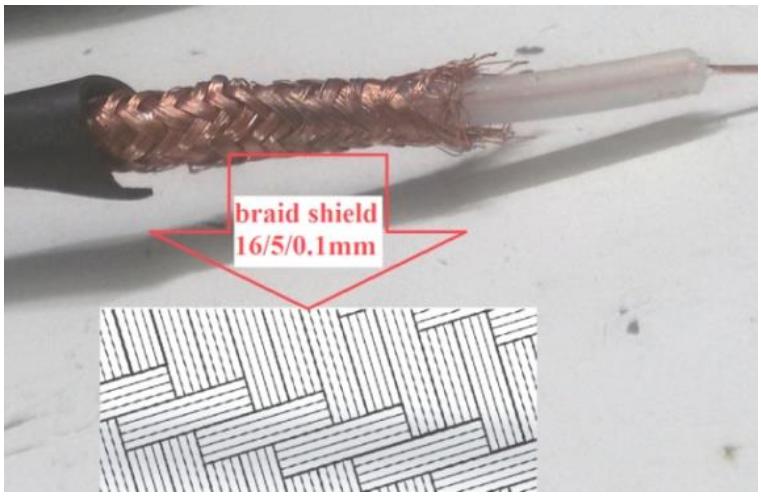


**Fig. 7. Coaxial cable components.**

**Table 4. Coordinates of probes.**

| Probe (E&H field) | Coordinate (x, y, z) in m |
|---|---|
| **A- Inside aircraft** | (22, 0.5, 0) |
| **B- Near win of aircraft** | (22, 2.95, 0) |
| **C- Outside aircraft** | (22, 3.5, 0) |

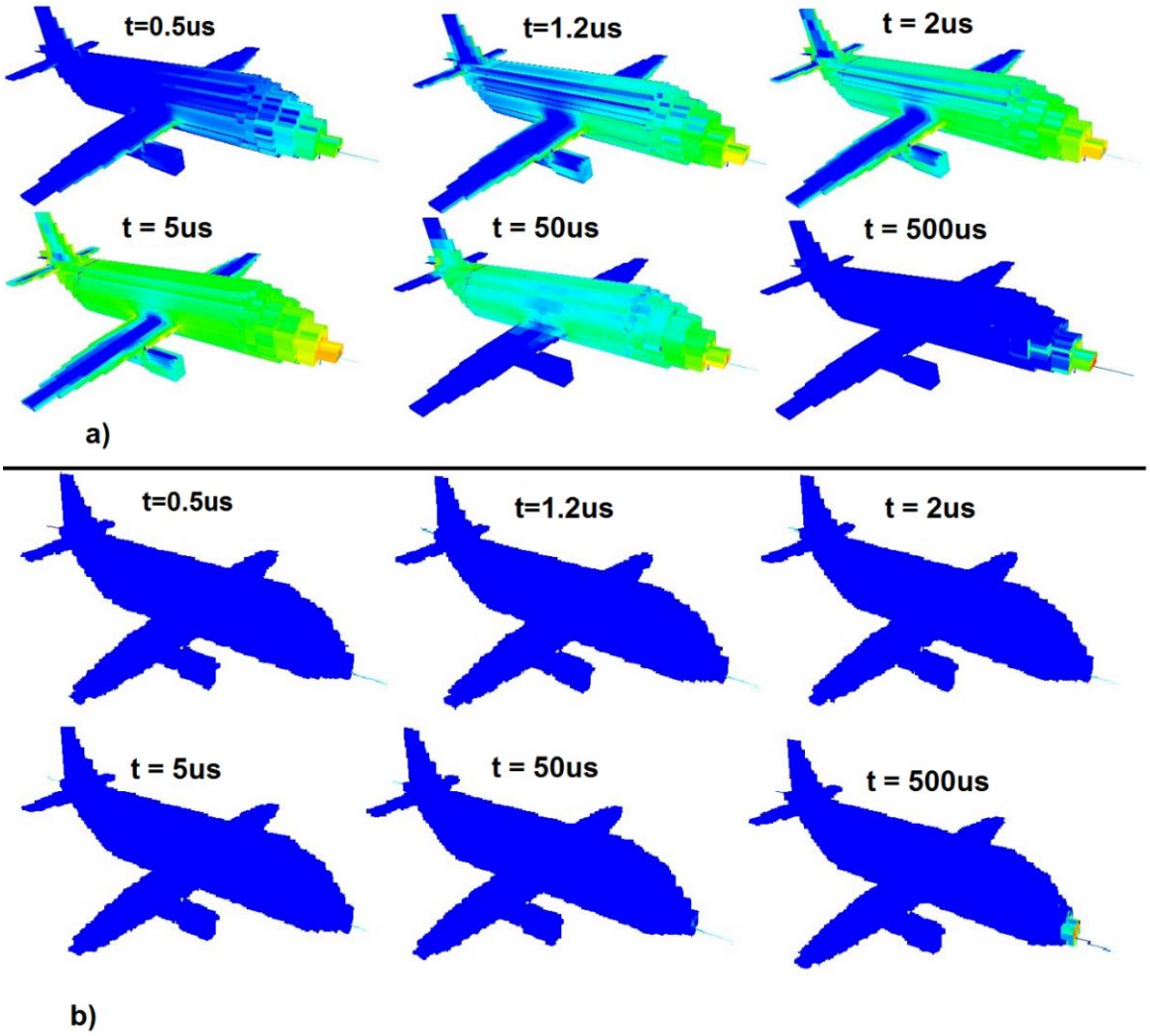


**Fig. 8. Expansion of surface current: a) CFC skin, and b) AL skin.**

equations and surface boundary conditions[34].

When a lightning channel attaches to an aluminum skin, localized melting can occur at the strike point. For CFC, however, resistive heating has an entirely different effect at entry and exit points. The damage may lead to a puncture. While aluminum can bend without breaking, CFC materials are rigid and prone to crushing. This damage is usually limited to the adjacency of the lightning attachment point. The aluminum model does not experience any significant temperature rise and remains almost at the ambient temperature.

### 7- 2- Magnetic and electric field strength

Electric and magnetic field strengths are measured at three probes, A, B, and C. The results in the time domain and frequency domain are displayed in Fig. 9 and Fig.10, as well as in Table 5 and Table 6.

Table 5 and Table 6 indicate the calculation of the shielding effectiveness of the aircraft skin. The shielding effectiveness is defined as the ratio of a field magnitude without the shield in place to the field magnitude with the shield in place.

The shielding effectiveness of electric and magnetic fields in dB is defined as follows:

$$SE_E = 20log\left|\frac{E_{outside}}{E_{transmitted}}\right| \tag{10}$$

$$SE_M = 20log\left|\frac{H_{outside}}{H_{transmitted}}\right| \tag{11}$$

As presented in Tables 5 and 6, the shielding effectiveness of the aluminum skin is significantly superior to that of the CFC skin.

### 7- 3- Induced current in coaxial cable

The induced current in coaxial cables is presented in Fig. 11.

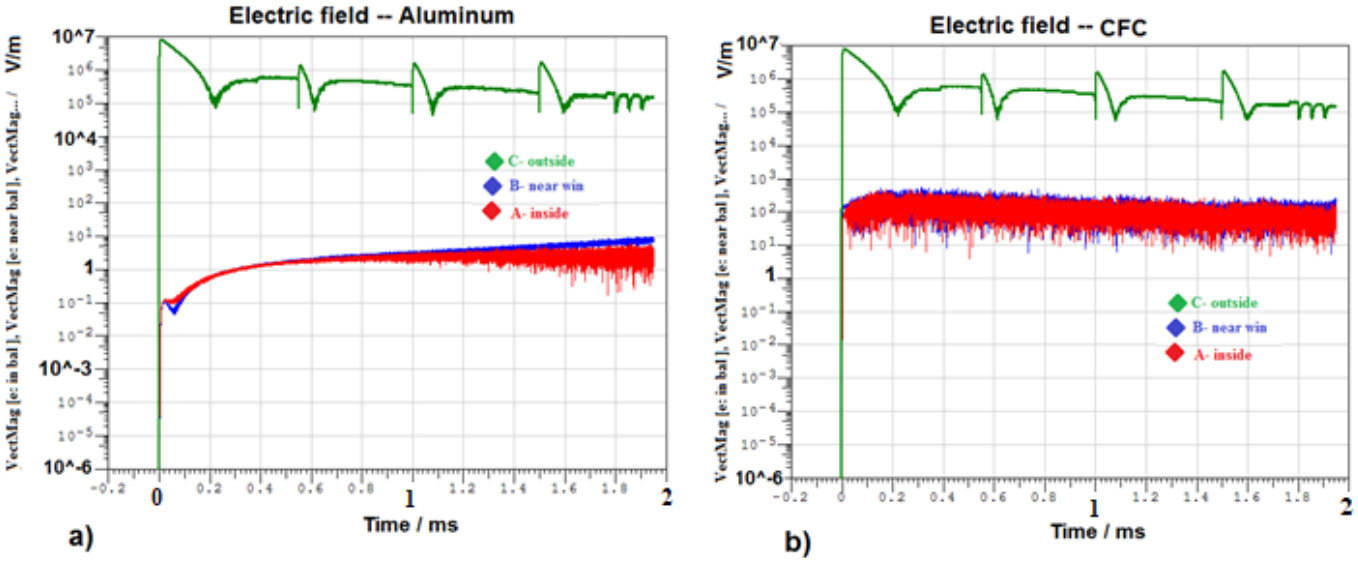


**Fig.9. Electric field strength in the time domain: a) AL, and b) CFC.**

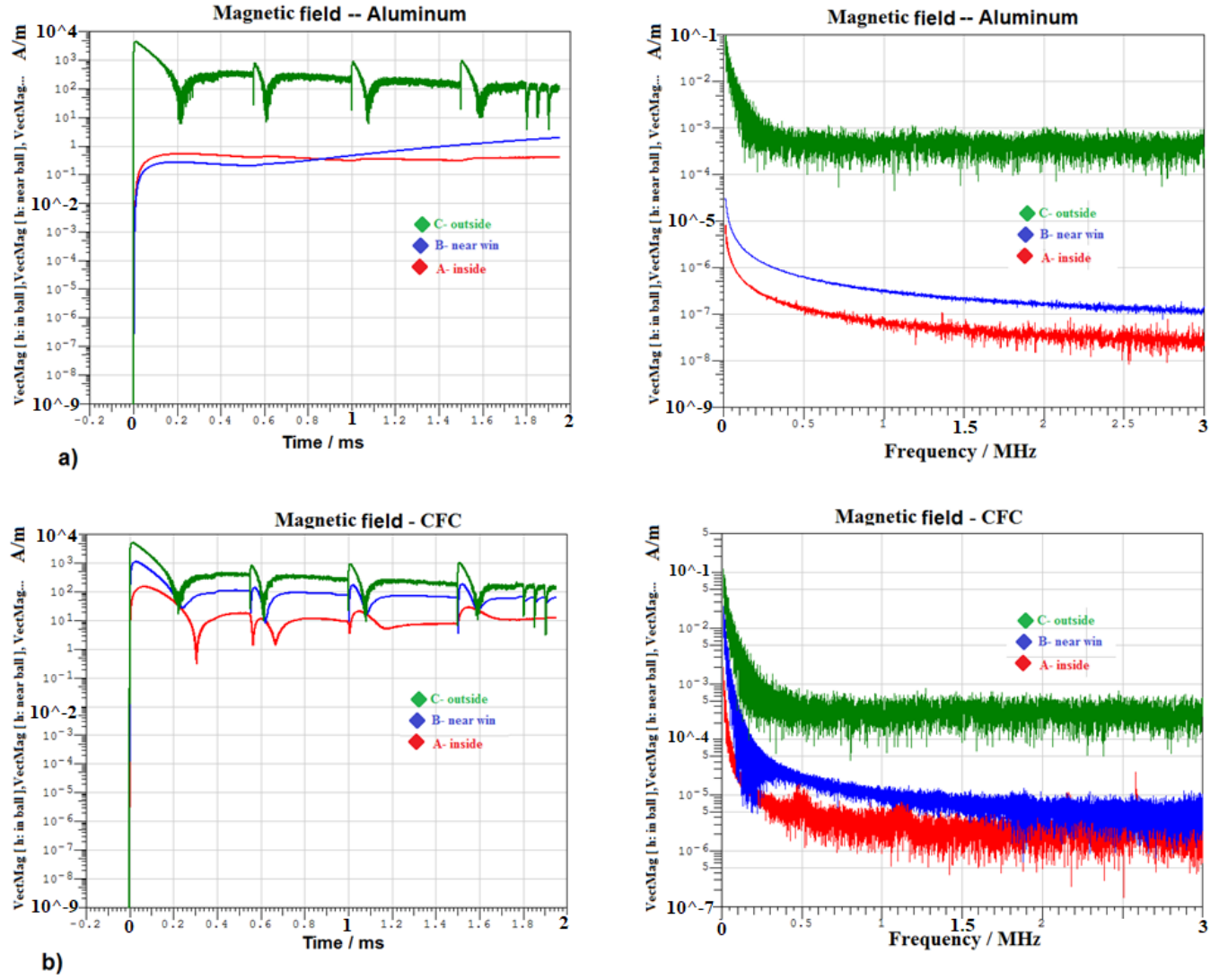


**Fig. 10. Magnetic field strength in time and frequency domain: a) AL, and b) CFC.**

**Table 5. Electric field strength.**

| Case | CFC | Aluminum |
|---|---|---|
| **Probe A** | 487V/m | 5.9V/m |
| **Probe B** | 553V/m | 9.6V/m |
| **Probe C** | 8.1MV/m | 8.1MV/m |
| **Shielding effectiveness ($SE_E$)** | 84.4 dB | 122.7 dB |

**Table 6. Magnetic field strength.**

| Case | CFC | Aluminum |
|---|---|---|
| **Probe A** | 150.4A/m | 527mA/m |
| **Probe B** | 1.1KA/m | 1.94A/m |
| **Probe C** | 5.16KA/m | 4.5KA/m |
| **Shielding effectiveness ($SE_M$)** | 30.7 dB | 78.6 dB |

**Table 7. Peak values of induced current in coaxial cables.**

| Coaxial cables | | Peak induced current | |
|---|---|---|---|
| | | Aluminum skin | CFC skin |
| **RG 174** | Shield screen | 9.9 mA | 13.3 A |
| | Inside wire | 23.9 uA | 32.2 mA |
| | Shielding effectiveness(dB) | 52.3 dB | |
| **RG-optional** | Shield screen | 9.6 mA | 13 A |
| | Inside wire | 236.3 uA | 320 mA |
| | Shielding effectiveness(dB) | 32.2 dB | |

The peak induced current is shown in Table 7.

As shown, the peak values of induced current in the inner wire of RG174 are lower than those in RG-optional. The shielding effectiveness of RG174 is 52.28 dB, while the RG-optional is 34.3 dB. It is worth noting that the protection offered by Aluminum skin is significantly superior to that of CFC skin.

## 8- Conclusion

This study quantified how the multi-stroke nature of a lightning flash affects the electromagnetic protection of aircraft. A full-wave TLM solver, enhanced with compact model surface impedance boundary conditions, was integrated with multi-stroke current waveforms generated in MATLAB that comply with MIL-STD-464A. The numerical methods of the electromagnetic effects, such as TLM, have the advantage of higher flexibility and lower costs with respect to the experimental approach. High investment and high-risk characteristics of experimental tests may cause a lot of inconvenience. Therefore, conducting the simulation of lightning protection is essential. The induced current, surface current density, and electric and magnetic field strengths were analyzed by comparing aluminum and composite fuselage structures. The present study could guarantee how much shielding is needed to achieve the best trade-off between minimizing weight and lightning-induced effects

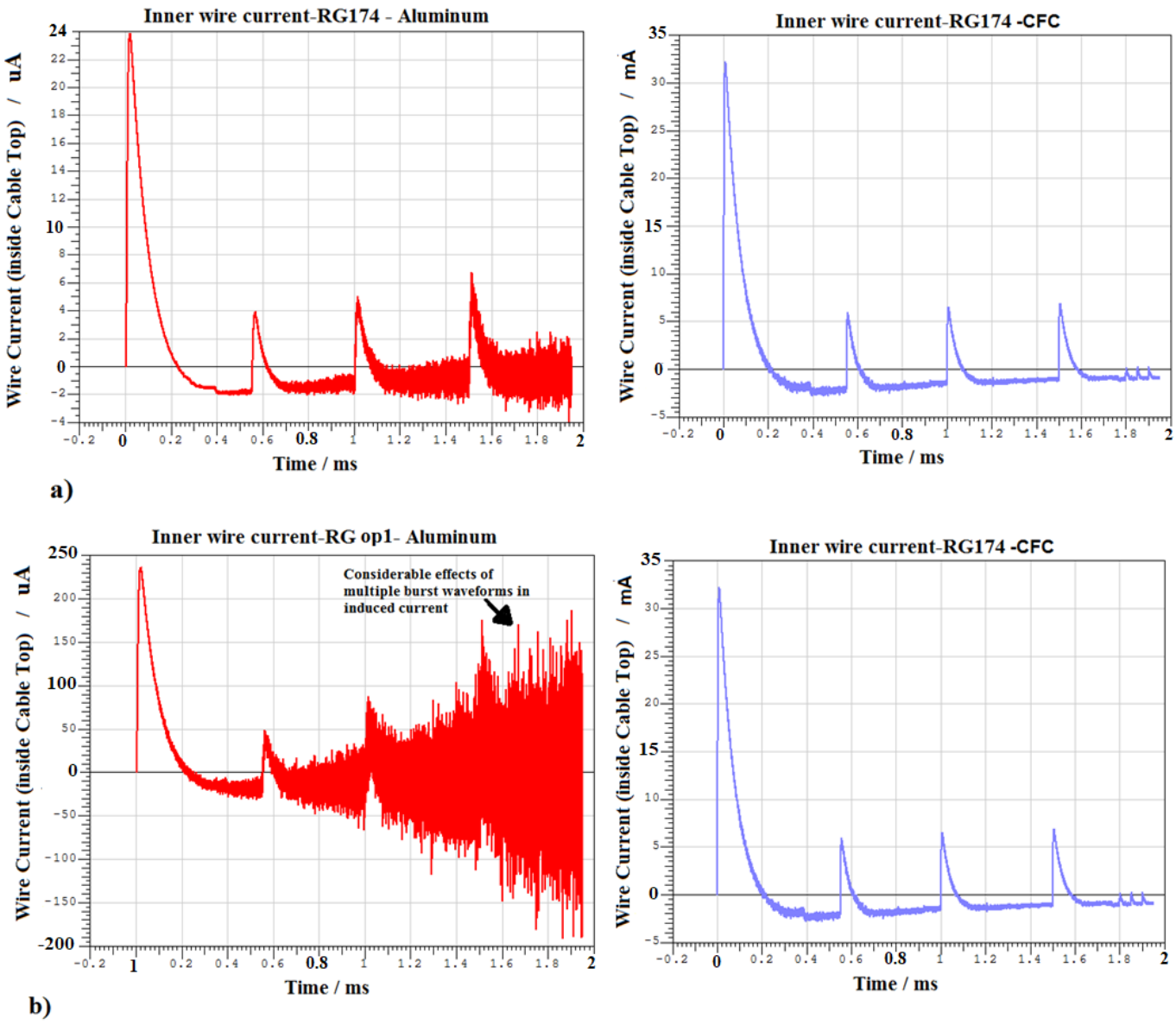


**Fig. 11. Induced current signal inside wire: a) RG174, b) RG-Optional.**

inside the aircraft. Finally, adding excessive shielding to the cable harnesses significantly increases the weight and reduces the routing flexibility. Although aluminum fuselage structures provide certain advantages in electromagnetic protection compared to carbon fiber composites (CFC), CFC materials are often preferred in contemporary aircraft design due to their superior strength-to-weight ratio. Consequently, CFC has become increasingly prevalent in modern aviation, despite the additional challenges it poses in terms of lightning protection. Results indicate that relying solely on single-stroke tests for certification is insufficient. Implementing conductive coatings, low-transfer-impedance cable shielding, and optimized cable routing are key strategies to ensure the reliability of avionics systems in modern fleets.

## References

[1] V. Kumar et al., "Factors affecting direct lightning strike damage to fiber reinforced composites: A review," Compos. Part B Eng., vol. 183, p. 107688, Feb. 2020, doi: 10.1016/J.COMPOSITESB.2019.107688.

[2] W. Adyatma, S. Hidayat, and R. Zoro, "Tropical Lightning Damage on Commercial Aircraft," in 2021 IEEE Aerospace Conference (50100), 2021, pp. 1–9. doi: 10.1109/AERO50100.2021.9438346.

[3] X. Ma, F. Wang, Z. Wang, Y. Li, and B. Xu, "Thermal dynamic damage of aircraft composite material suffered from lightning channel attachment based on moving mesh method," Compos. Sci. Technol., vol. 214, p. 109003, Sep. 2021, doi: 10.1016/J.COMPSCITECH.2021.109003.

[4] F. Padoan, D. Clark, A. Haddad, C. Karch, and P. Westphal, "Initiation of Electrical Discharge at the Triple Junction of the Lightning Protection of an Aircraft Radome," IEEE Electr. Insul. Mag., vol. 39, no. 1, pp. 6–16, 2023, doi: 10.1109/MEI.2023.9999633.

[5] H. Neyshabouri and M. Niasati, "Transient investigations on lightning overvoltages applied on oil tanks roof considering grounding configurations," Electr. Eng., vol. 104, no. 4, pp. 2437–2447, 2022, doi: 10.1007/s00202-021-01452-w.

[6] Y. S. Kang, S. W. Park, J. S. Roh, and R. S. Myong, "Computational Investigation of Effects of Expanded Metal Foils on the Lightning Protection Performance of a Composite Rotor Blade," Int. J. Aeronaut. Sp. Sci., vol. 22, no. 1, pp. 203–221, 2021, doi: 10.1007/s42405-020-00288-1.

[7] W. Matsunaga, S. Imai, Y. Mizutani, T. Yasuoka, and A. Todoroki, "Estimation of the moisture absorption rate of carbon fiber reinforced plastic using electromagnetic induction testing," Compos. Part A Appl. Sci. Manuf., vol. 177, p. 107934, Feb. 2024, doi: 10.1016/J.COMPOSITESA.2023.107934.

[8] U. Alkasi, "Analysis and Comparison of Lightning Indirect Effects in Aluminum, Composite Fiber Reinforced Plastic and Expanded Copper Foil embedded CFRP Aircraft with EMA3D," in 2023 7th International Electromagnetic Compatibility Conference (EMC Turkiye), 2023, pp. 1–8. doi: 10.1109/EMCTurkiye59424.2023.10287521.

[9] S.-Y. Kim, J.-S. Park, and W.-S. Lee, "Development and verification of indirect lightning-induced transient protection circuit for avionics system," Appl. Comput. Electromagn. Soc. J., vol. 36, no. 6, pp. 670–675, 2021, doi: 10.47037/2020.aces.j.360608.

[10] J. Jo, Y. Kim, D. Kim, H. Lee, and R. S. Myong, "Effect of Shielding and Drain Wire on Lightning-Induced Currents in Rotorcraft Cables," IEEE Trans. Electromagn. Compat., vol. 64, no. 6, pp. 2015–2023, 2022, doi: 10.1109/TEMC.2022.3198697.

[11] H. P. Rimal et al., "Protection From Indirect Lightning Effects for Power Converters in Avionic Environment: Modeling and Experimental Validation," IEEE Trans. Ind. Electron., vol. 68, no. 9, pp. 7850–7862, 2021, doi: 10.1109/TIE.2020.3013794.

[12] M. Wyatt, D; & Tooley, Aircraft Electrical and Electronic Systems, 2nd ed. Routledge, 2018. doi: 10.1201/9780429504228.

[13] T. Akay and C. Tarhan, "The effect of global warming and climate changes on aircraft accidents between 2010-2022," Aircr. Eng. Aerosp. Technol., vol. ahead-of-p, no. ahead-of-print, Jan. 2023, doi: 10.1108/AEAT-03-2023-0081.

[14] L. Nikšić and E. Arıkan Öztürk, "Analysis of ATC-related aviation accidents and incidents," Aircr. Eng. Aerosp. Technol., vol. 95, no. 6, pp. 890–898, Jan. 2023, doi: 10.1108/AEAT-03-2022-0078.

[15] STD MIL, 464 A Electromagnetic Environmental Effects Requirements for systems. US Department of Defense, 2002.

[16] L. Chemartin et al., "Direct Effects of Lightning on Aircraft Structure Analysis of the Thermal, Electrical and Mechanical Constraints," Aerosp. Lab, no. 5, pp. 1–15, 2012, [Online]. Available: httpshal.sciencehal-01184416

[17] P. Lalande and A. Delannoy, "Numerical Methods for Zoning Computation," Aerosp. Lab, no. 5, pp. 1–10, 2012, [Online]. Available: https://hal.science/hal-01184414

[18] H. Neyshabouri and M. Niasati, "Analysis of the electromagnetic effects on the large floating roof oil tanks by nearby lightning strike based on TLM," J.Electrostat., vol. 129, no. 4, pp. 103927, 2024, doi: 10.1016/j.elstat.2024.103927.

[19] A. Broc et al., "A lightning swept stroke model: A valuable tool to investigate the lightning strike to aircraft," Aerosp. Sci. Technol., vol. 10, no. 8, pp. 700–708, Dec. 2006, doi: 10.1016/J.AST.2005.10.008.

[20] CST, Reference Manual. Computer Simulation Technology. GmbH, 2020.

[21] J. S. L. Colqui, L. C. T. Eraso, P. T. Caballero, J. P. Filho, and S. Kurokawa, "Implementation of Modal Domain Transmission Line Models in the ATP Software," IEEE Access, vol. 10, pp. 15924–15934, 2022, doi: 10.1109/ACCESS.2022.3146880.

[22] M. N. Sadiku, Numerical Techniques in Electromagnetics with MATLAB, Third Edit. CRC press, Boca Raton, 2009. doi: https://doi.org/10.1201/9781315222622.

[23] J. S. Odeyemi, A. Vukovic, T. M. Benson, and P. D. Sewell, "A Complex Domain Mapping of the SCN for an Effective PML Implementation in TLM," IEEE Open J. Antennas Propag., vol. 1, pp. 126–135, 2020, doi: 10.1109/OJAP.2020.2986293.

[24] O. Gassab et al., "Transmission Line Modeling and Crosstalk Analysis of Multibraided Shielded TWP/Twinax Cables," IEEE Trans. Electromagn. Compat., vol. 64, no. 5, pp. 1560–1573, 2022, doi: 10.1109/TEMC.2022.3179512.

[25] M. Moumou, S. El Adraoui, K. Mounirh, M. Kanjaa, and M. Khalladi, "Efficient ADE-TLM scheme for modeling Drude based graphene in terahertz spectrum," Prog. Electromagn. Res. Lett., vol. 112, pp. 119–126, 2023, doi: 10.2528/pierl23060904.

[26] M. Apra, M. D'Amore, K. Gigliotti, M. S. Sarto, and V. Volpi, "Lightning Indirect Effects Certification of a Transport Aircraft by Numerical Simulation," IEEE Trans. Electromagn. Compat., vol. 50, no. 3, pp. 513–523, 2008, doi: 10.1109/TEMC.2008.927738.

[27] M. Zhang and Z. Huang, "Transient current burst analysis induced in cable harness due to direct lightning strike on aircraft," in 2010 Asia-Pacific International Symposium on Electromagnetic Compatibility, 2010, pp. 1197–1200. doi: 10.1109/APEMC.2010.5475508.

[28] F. S. Wang, X. S. Yu, S. Q. Jia, and P. Li, "Experimental and numerical study on residual strength of aircraft carbon/epoxy composite after lightning strike," Aerosp. Sci. Technol., vol. 75, pp. 304–314, Apr. 2018, doi: 10.1016/J.AST.2018.01.029.

[29] K. Patra, S. Cheruvalath, S. Dhar, B. P. Nayak, A. Gupta, and J. Hansen, "Surrogate Modeling for Predicting Shielded Cable Emissions," IEEE Trans. Electromagn.

Compat., vol. 65, no. 1, pp. 249–256, 2023, doi: 10.1109/TEMC.2022.3225631.

[30] K. Santos et al., "Evaluation of Surface Transfer Impedance of Coaxial Cables," IEEE Lat. Am. Trans., vol. 18, no. 03, pp. 598–603, 2020, doi: 10.1109/TLA.2020.9082732.

[31] O. Gassab, S. Bouguerra, L. Zhou, and W.-Y. Yin, "Efficient Analytical Model for the Transfer Impedance and Admittance of Noncoaxial/Twinax Braided–Shielded Cables," IEEE Trans. Electromagn. Compat., vol. 62, no. 6, pp. 2725–2736, 2020, doi: 10.1109/TEMC.2020.2996204.

[32] P. Hu et al., "Measurement Techniques for Electromagnetic Shielding Behavior of Braided-Shield Power Cables: An Overview and Comparative Study," Meas. Sci. Rev., vol. 19, no. 5, pp. 213–221, 2019, doi: doi:10.2478/msr-2019-0028.

[33] M. Schoeman, E. A. Attardo, and J. S. Castany, "Recent Advances to the Feko Integrated Cable Harness Modeling Tool," in 2019 International Symposium on Electromagnetic Compatibility - EMC EUROPE, 2019, pp. 1071–1075. doi: 10.1109/EMCEurope.2019.8871980.

[34] C. A. Balanis, Advanced Engineering Electromagnetics. Hoboken, NJ: Wiley, 2012.

**HOW TO CITE THIS ARTICLE**

*H. Neyshabouri, M. Niasati, Evaluation of Lightning Multiple Strokes Nature on Aircraft Avionic Equipment Performance Based on TLM, AUT J. Elec. Eng., 57(3) (2025) 485-498.*

**DOI:** 10.22060/eej.2025.23758.5633